COBEM 2021 26th International Congress of Mechanical Engineering
ABCM Associação Brasileira de Engenharia e Ciências Mecânicas
November 22-26, 2021, Virtual Congress, Brazil

COB-2021-2152
DETECTION OF SUBSEA GAS LEAKAGES VIA COMPUTATIONAL FLUID DYNAMICS AND CONVOLUTIONAL NEURAL NETWORKS

Gustavo Luís Rodrigues Caldas†
gustavo.caldas@eq.ufrj.br

Thiago Ferreira Bernardes Bento
Programa de Pós-Graduação em Engenharia Mecânica e Tecnologia de Materiais, Centro Federal de Educação Tecnológica Celso Suckow da Fonseca (Cefet/RJ). Rua General Canabarro 485, Rio de Janeiro, RJ, Brazil.
tbento@id.uff.br

Roger Matsumoto Moreira
Escola de Engenharia, Universidade Federal Fluminense. Rua Passos da Pátria 156, bl.D, sl.563A, Niterói, RJ, Brazil.
rmmoreira@id.uff.br

Maurício Bezerra de Souza Júnior†
†Programa de Pós-Graduação em Engenharia de Processos Químicos e Bioquímicos, Escola de Química, Universidade Federal do Rio de Janeiro. Av. Athos da Silveira Ramos 149, bl.E, sl.207, Ilha do Fundão, Rio de Janeiro, RJ, Brazil.
mbsj@eq.ufrj.br

Abstract. *Gas leakage can generate a considerable number of losses in environmental and economic terms. Constant monitoring of deep-water wells is an important safety tool to enable fast and proper responses, prevent the conditions' aggravation, and avoid unnecessary costs. A monitoring approach is to install video cameras in the subsea environment to track possible leaks. Automation of the process is possible by using image analyses algorithms. In this context, convolutional neural network (CNN) is a methodology part of the Artificial Intelligence framework, capable of extracting relevant features from images. The objective of this work is to develop a tool to detect fault in subsea pipelines using the presence of bubbles in the images as an indicator. Computational Fluid Dynamics (CFD) simulations were developed aiming to reproduce subsea gas leakages. The volume of fluid (VOF) method is employed to model the two-phase gas-liquid flow, in which bubbles are released into stagnant water with different leakage flow rates and orifice diameters. The frames obtained from the simulation images served as input to the CNN. The methodology is intended to distinguish between a scenario of normality (no leakage/bubble) and abnormality (leakage/bubble). The classification task of bubble presence or absence performed by the CNN reported high accuracy (99%). No false alarms (fall-outs) in all sets, high specificity (true negative rate) and precision of the classifier were found. Good accuracy supports its potential as fault detector. This approach could be extended to other applications in the field of Fault Detection and Diagnosis, not limited to the present scope.*

Keywords: *gas leakage, Convolutional Neural Networks, subsea pipelines, CFD, fault detection.*

1. INTRODUCTION

Subsea oil well drilling activities and their transportation by pipelines are susceptible to incidents of significant environmental and economic impact, especially if in decommissioning state and/or after a long time of service (Nazir *et al.*, 2008). Olsen and Skjetne (2016) classify these incidents in seep, which could occur naturally or due to drilling activity; leaks, that may not be detected if of small scale; rupture, an event of greater impact, but with control; and blowout, a major release with loss of control. Eventually, cracks in well equipment and pipelines may evolve from small leaks to large material releases. Containing the leakage on early stage can be the key to avoid a disaster. Therefore, the use of risk assessment techniques is justified, one of which is ROVs (remotely operated vehicles), which register these events *in loco*. With the leakage visualization, a fast and safe response can be performed, allowing the technicians to make a qualitative evaluation of the situation, especially for events that pose great danger. However, the decision-making process of intervention based on video images is still totally qualitative, delivering no quantitative information about the leakage, such as flow rates. Fault detection and diagnosis (FDD) have become a central point to the process industry because the ramping operations complexity demands loss prevention and environmental safety maintenance. In the FDD terminology, fault is a system state in which a deviation from the accepted operational range occurs. Detection denotes whether the fault

has occurred, while diagnosis points out which fault is, its type, and its magnitude (Isermann, 2006; Chiang *et al.*, 2001). Venkatasubramanian divided the methods into three: quantitative model-based (Venkatasubramanian *et al.*, 2003b), qualitative models and search strategies (Venkatasubramanian *et al.*, 2003a), and process history based (Venkatasubramanian *et al.*, 2003c). One potential technique in this context is artificial neural network (ANN), a data-driven approach that recognizes patterns without modelling the system.

More precisely, ANNs are subsymbolic processing structures that vaguely resemble brain learning operation. They integrate the machine learning algorithms (ML). Information is learned through the connections between inputs and outputs in the nodes (neurons) of the ANN, organized in layers, whose dynamic response is given by external stimuli (adjustment of weights and activation function). The first neural networks that gained massive use were the multilayer perceptron (MLP) networks (de Souza Jr., 1993). More recently, these techniques have evolved to deep learning, in which there are more layers, requiring fewer data pre-processing (LeCun *et al.*, 2015).

Convolutional neural networks (CNNs) have been increasingly used in image processing, solving more efficiently and speedily classification problems (Krizhevsky *et al.*, 2012; LeCun *et al.*, 1989), object detection (Sun *et al.*, 2018), segmentation (Schäfer *et al.*, 2019), and, even, identification of pipeline failures by visual inspection in subsea environments (Petraglia, 2017). CNNs can accommodate the large amount of information comprised in the form of tensors, including not only images, but also signal analysis from machinery (Jiao *et al.*, 2020; Zhang *et al.*, 2020; Cheng *et al.*, 2021), spatial and time-domain data transformed (Wu and Zhao, 2018; Ge *et al.*, 2021), acoustic information (Wang *et al.*, 2019) and speech (Abdel-Hamid *et al.*, 2014).

In the present era, the industry is entering the fourth industrial revolution, i.e., an integration of cyber-physical systems and the advancement of communication and information systems between machines, sensors, and devices. Furthermore, a tremendous amount of process knowledge is collected, enabling an immediate fault detection and diagnosis. Therefore, convolutional neural networks can support the decision-making process, as they are capable of coping the large amounts of image parameters (pixels) and extracting their features, outperforming traditional image processing techniques. In this sense, the aim of this work is to classify synthetic gas leakage data (obtained from CFD simulations) employing convolutional neural network, an innovation in the field of FDD. CFD results for different flow conditions are employed as the input data of the implemented CNN algorithm. This paper is divided as follows: the investigation development, including evaluation metrics and the models used, is presented in Section 2; the results obtained from the experiments are discussed in Section 3; finally, Section 4 summarizes our main conclusions and future perspectives.

2. METHODOLOGY

First, Computational Fluid Dynamics (CFD) techniques were applied to reproduce gas leakages. To simplify our model a two-phase air-water flow was chosen, with bubbles being released into stagnant water for different velocities and orifice diameters.

2.1 CFD Formulation

The unsteady incompressible viscous flow is modeled with momentum and mass being conserved. Continuity and the unsteady RANS (Reynolds-Averaged Navier-Stokes) equations are then satisfied in the fluid domain,

$$\frac{\partial \bar{u}_i}{\partial x_i} = 0 \qquad \frac{\partial \bar{u}_i}{\partial t} + \frac{\partial \left(\bar{u}_i \bar{u}_j\right)}{\partial x_j} = f_i - \frac{1}{\rho}\frac{\partial \bar{P}}{\partial x_i} + \nu \frac{\partial^2 \bar{u}_i}{\partial x_j^2} - \frac{\partial \left(\overline{u_i' u_j'}\right)}{\partial x_j} \tag{1}$$

where the subscript i (or j) indicates the direction of an orthogonal axes system; t is time; x_i is the position; $u_i \left(= \bar{u}_i + u_i'\right)$ is the fluid velocity decomposed, respectively, in mean and fluctuating velocities; f_i is the acceleration due to gravity; ρ is the fluid density; $\bar{P}$ is the mean dynamic pressure; ν is the kinematic viscosity. To solve the closure problem of turbulence, the classical $\kappa - \varepsilon$ model is used (Launder and Spalding, 1974),

$$\frac{\partial(\rho\kappa)}{\partial t} + \frac{\partial(\rho\kappa\bar{u}_i)}{\partial x_i} = \frac{\partial}{\partial x_j}\left(\frac{\mu_T}{\sigma_\kappa}\frac{\partial \kappa}{\partial x_i}\right) + 2\mu_T \bar{E}_{ij} : \bar{E}_{ij} - \rho\varepsilon \tag{2}$$

$$\frac{\partial(\rho\varepsilon)}{\partial t} + \frac{\partial(\rho\varepsilon\bar{u}_i)}{\partial x_i} = \frac{\partial}{\partial x_j}\left(\frac{\mu_T}{\sigma_\varepsilon}\frac{\partial \varepsilon}{\partial x_i}\right) + 2\mu_T C_{1\varepsilon}\frac{\varepsilon}{\kappa}\bar{E}_{ij} : \bar{E}_{ij} - \rho C_{2\varepsilon}\frac{\varepsilon^2}{\kappa} \tag{3}$$

where $\kappa \left(= \frac{1}{2}\left|\overline{u_i'^2}\right|^2\right)$ is the turbulent kinetic energy; ε is the rate of dissipation; $\mu_t \left(= \rho C_\mu \frac{\kappa^2}{\varepsilon}\right)$ is the turbulent viscosity. The stress tensor $\bar{E}_{ij}$ is defined by,

$$\bar{E}_{ij} = \frac{1}{2}\left(\frac{\partial \bar{u}_i}{\partial x_j} + \frac{\partial \bar{u}_j}{\partial x_i}\right) \tag{4}$$

where the other constants are: σ_κ = 1.00; σ_ε = 1.30; C_μ = 0.09; $C_{1\varepsilon}$ = 1.44; $C_{2\varepsilon}$ = 1.92.

Air-water interface is modeled via the VOF (Volume of Fluid) method, proposed by Hirt and Nichols (1981),

$$\frac{\partial \Phi}{\partial t} + u_i \frac{\partial \Phi}{\partial x_i} = 0 \tag{5}$$

where Φ represents the volume fraction: $\Phi = 0$ when the cell has only air inside; $\Phi = 1$ when the cell is full of water; $0 < \Phi < 1$ when there is a fluid interface in the cell.

For simplicity, computations were developed in a two-dimensional fluid domain with reduced dimensions, 40 cm of height and 20 cm of width . A non-slipping condition was applied at all boundaries, except at the top, where a free-surface condition with atmospheric pressure was used. Cartesian coordinates are defined by setting, respectively, the x and y-axis in the horizontal and vertical directions. Air bubbles were emitted at the mid-bottom of the fluid domain with different orifice diameters d and velocities v, as shows Tab. 1.

Table 1: Leakage parameters.

Condition #	d (mm)	v (m/s)
1	0.5	0.25
2		0.63
3		1.0
4	1.0	0.24
5		0.37
6		0.50
7	5.0	0.02
8		0.06
9		0.09

The initial value problem is solved by the CFD package ANSYS Fluent 2019, release 3, which makes use of the finite volume method. The mesh was refined near the leakage orifice, with a total of 3×10^5 discretization elements. According to the leakage parameters specified in Tab. 1, time intervals of 0.5 and 0.6 ms were employed for a total simulation time of 3 s. All the computations were carried out on a 64 bit, 3.40 GHz Intel Core i7-8700 processor with 16 Gb of RAM.

2.2 Convolutional Neural Network used for Classification

The post-processing step created a series of videos according to the conditions in Table 1. This series of videos were cropped and automatic snapshots using VLC Video Player were taken in order to feed the image processing tools and the neural networks. Since each video has frame ratio of 30 frame per second, but each one has different length, different recording ratios were employed in order to maintain an uniform dataset as described in Tab. 2. A total number of 3409 images of size 48 x 128 pixels were generated. Starting at the height 18 mm of the water column, the area examined comprised 43 mm x 116 mm in the real scale. The recording ratio is defined as the ratio in which the frame is taken. When recording ratio is equal to one, all frames are captured. On the other hand, when the recording ratio is equal to three, one out of three frames are captured.

Table 2: Video and dataset specifications.

Condition #	Video length	Recording ratio	Number of images generated
1	00:00:49	3	394
2	00:00:16	1	394
3	00:00:16	1	395
4	00:00:13	1	330
5	00:00:13	1	329
6	00:00:16	1	395
7	00:00:17	1	425
8	00:00:41	3	332
9	00:00:17	1	414

A classification network was developed to distinguish between a scenario of normality (no leakage/bubble) and abnormality (leakage/bubble). The aim is to develop a tool to detect any leakage in the pipelines. To train the neural network prediction model, a target must be defined, in this case for a binary classification, one (bubble presence) or zero (bubble absence). The images were imported into grayscale using the Scikit-Image processing library (Buitinck *et al.*, 2013). No data pre-processing was necessary to be performed, except scaling the input according to the following equation:

$$x' = \frac{x}{255} \tag{6}$$

The next step is to split randomly the dataset into train, validation and test. Train set is used to fit and adjust the weights, and the model is submitted to evaluation using validation set while adjusting the hyperparameters. As the fit process develops, both become biased, therefore it is necessary to check the robustness of the model against the test set at the end, which was not employed for training. Here the proportion adopted was 60 %, 24 % and 16 %, respectively.

The data were fed to the convolutional neural networks developed in the Keras environment using Python, backended by Tensorflow. The architecture employed two convolutional layers, as expressed in Tab. 3. Both convolutional layers have kernel size of 3 x 3 and L2 kernel regularizer factor of 0.01, in which the first one has 32 filters and the second one has 64 filters. Pooling layers have size 2 x 2 with stride 2.

Table 3: Classifier CNN architecture.

Layer (type)	Output Shape	Number of parameters
Input	(128, 48, 1)	-
Convolutional 2D + ReLU	(126, 46, 32)	320
Max Pooling 2D	(63, 23, 32)	0
Batch Normalization	(63, 23, 32)	128
Convolutional 2D + ReLU	(126, 46, 32)	18496
Max Pooling 2D	(30, 10, 64)	0
Flatten	(19200)	0
Dropout 20 %	(19200)	0
Dense Layer 1 + ReLU	(16)	307216
Dense Layer 2 + Sigmoid	(1)	17
	Total	326,113 trainable+ 64 non-trainable

The units employing activation function uses the rectified linear unit - ReLU (Eq. 7a) and the sigmoid function (Eq. 7b). ReLU increases computational efficiency because it is less subject to the vanishing gradient problem (Glorot *et al.*, 2011). The output of a sigmoidal activation is restrict to the range of 0 to 1, representing a probability score. It maps the event of fault occurrence according to the value output: if it is more than 50 %, then the event is classified as abnormal situation (bubble).

$$\mathrm{ReLU(x)} = max(0, x) \tag{7a}$$

$$\mathrm{S(x)} = \frac{1}{1 + e^{-x}} \tag{7b}$$

As the loss function to be minimized, the average binary cross-entropy for N samples was employed (Eq. 8a). In this notation, q represents the estimated probability, and p the true probability for each class c. Setting the notation as y and $\hat{y}$ for the true and predicted outputs, respectively, then for a binary case the follows hold: $p \in \{y, 1-y\}$ and $q \in \{\hat{y}, 1-\hat{y}\}$

Accuracy was also monitored as a metric (Eq. 8b), which computes the rate of true positives and true negatives over the total number of samples. The optimizer employed was Adam (Kingma and Ba, 2017). The batch size number corresponds to 128 and the maximum number of epoches allowed is equal to 100.

$$\mathrm{CE(p, q)} = -\frac{1}{N}\sum_{n=1}^{N}\sum_{c} p_{n,c}\log q_{n,c} = -\frac{1}{N}\sum_{n=1}^{N}[y_n \log \hat{y_n} + (1-y_n)\log(1-\hat{y_n})] \tag{8a}$$

$$\mathrm{ACC} = \frac{1}{N}\sum_{n=1}^{N}[\hat{y_n} = y_n] \tag{8b}$$

3. RESULTS AND DISCUSSION

3.1 CFD Model

The different operational conditions generated a series of videos, which is a visual representation of the phenomena occurring in the reduction model, e.g. the numeric diameter d_b represented in Fig. 1 and in Tab. 4. For each case, equivalent spherical diameters d_b were estimated based on the total air volume per length V and the number of bubbles N released within the water column, such that $d_b = \left(\frac{4}{\pi}\frac{V}{N}\right)^{1/2}$ (see last column of Tab. 1). The results were compared to experimental data, and a good agreement was found for low leakage velocities (Calazan *et al.*, 2021).

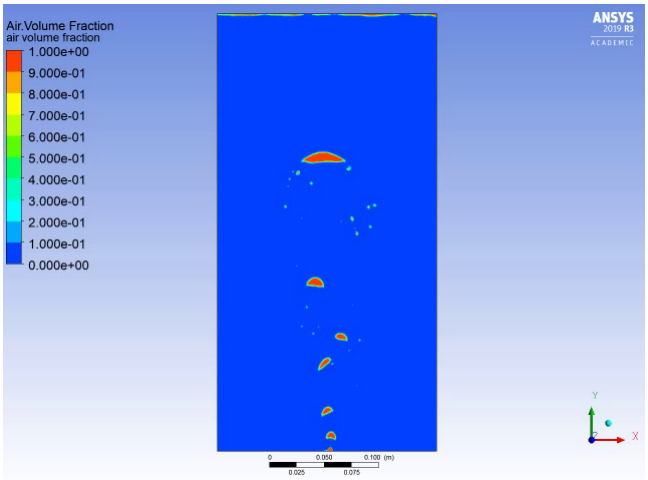

Figure 1: A CFD snapshot of released air bubbles (in red) in a water column (in blue).

Table 4: Numerical diameter according to the leakage parameters.

Condition #	d (mm)	v (m/s)	d_b (mm)
1	0.5	0.25	6.45
2		0.63	7.22
3		1.0	7.69
4	1.0	0.24	6.37
5		0.37	6.46
6		0.50	7.28
7	5.0	0.02	6.70
8		0.06	8.05
9		0.09	8.11

3.2 Classifier CNN

A straightforward manner to assess classification done by the CNN is the confusion matrix, illustrated for each data set (Fig. 2). In a binary classification problem, there are four possible outcomes: if the input is positive for bubble presence and the algorithm regards it as positive, then it is denoted as true positive (TP); if there is no bubble on the image and the output is also negative, this is called true negative (TN); if the data is positive, but the prediction is negative, it is a false negative (FN); conversely, it is a false positive (FP) (Tharwat, 2020; Sokolova and Lapalme, 2009). No false positives reported indicates that the classifier does not generate false alarms (or fall-outs) in none of the sets. Also, it is an evidence for the CNN's high specificity (TN rate) and precision. For the FDD, this fact brings reliability to the operator, who would immediately recognize the need of taking further actions.

Furthermore, this network possesses a high sensitivity (or recall) regarding the positive detection, with a miss rate of only 0.2 %. Hence, it can be affirmed that this classifier network has a good predictability regarding bubble detection. Investigating the false negatives gives an indication of the CNN's capacity. Fig. 3 shows the incorrect predictions from training. On the bottom, the bubbles are in white as highlighted in the red squares. The missed detection in training was due to the choice of assigning an image as "with bubble" as soon the leakage shows off. Thereby a very small piece of bubble was missed out by the neural network.

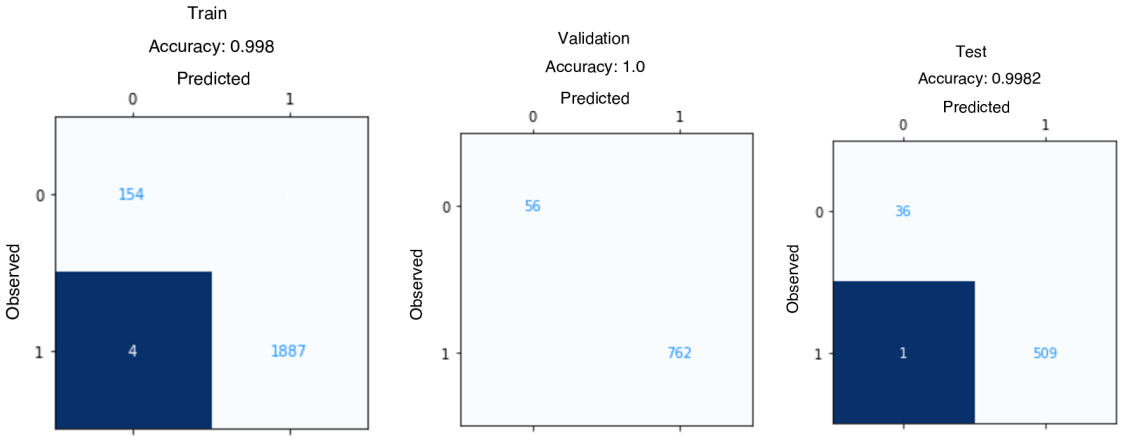

(a) (b) (c)

Figure 2: Confusion matrices for the following datasets: (a) Train (b) Validation (c) Accuracy.

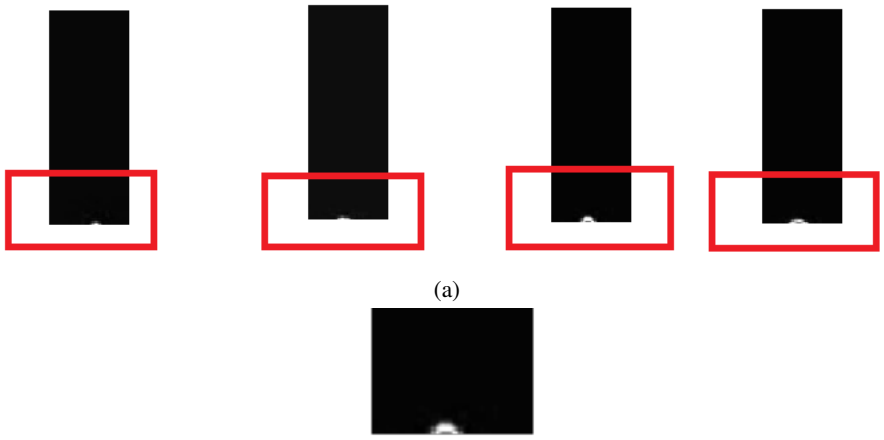

(a)

(b)

Figure 3: (a) Incorrect predictions from training, (b) from (a), third red square in detail.

The progress of the neural network during the epochs is shown at Fig. 4. A fast decrease of both validation and training loss can be seen during the first twenty epochs. However, the algorithm converges only after one-hundred iterations, the maximum allowed. Since the minimum difference adopted in loss between epochs for early stopping was 1.0 x 10^{-4}, the analysis took more time (around twenty minutes) than if softer conditions were applied, which probably would have stopped earlier. There is, therefore, a clear trade-off between computational time and accuracy.

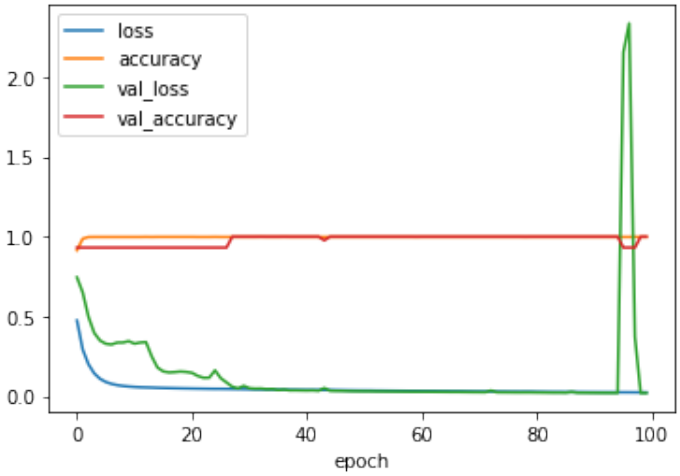

Figure 4: Classifier CNN: Loss and metrics against the epochs.

4. CONCLUSION

A novel methodology using deep learning was presented, using a classifier tool. The classifier provides precise and sensible computational vision, and it is capable of differentiating between images with and without bubbles. Good accuracy supports it as a potential fault detector. It could be extended to other applications in the field of Fault Detection and Diagnosis based on images, but not restricted to the presented scope.

For future works, the simulation could be broadened to different gas leakage scenarios, but still within minor leak events, since the concept is to work on the prevention of the leak worsening rather than remediation. As a continuation of this work, it is suggested to process experimental data in order to validate the methodology.

5. ACKNOWLEDGEMENTS

The authors from Universidade Federal do Rio de Janeiro acknowledge the financial support granted by the National Agency of Petroleum, Natural Gas, and Biofuels – ANP through the Program of Human Resources for the Oil, Gas & Biofuels Industry (PRH). PRH is funded by oil companies qualified in the R&D and Innovation clause from the ANP Resolution 50/2015 (process number: 041319). The authors from Universidade Federal Fluminense and Centro Federal de Educação Tecnológica Celso Suckow da Fonseca acknowledge the financial support from PETROBRAS (termo de cooperação PETROBRAS/UFF/FEC 5900.0113248.19.9).

6. REFERENCES

Abdel-Hamid, O., Mohamed, A.r., Jiang, H., Deng, L., Penn, G. and Yu, D., 2014. "Convolutional Neural Networks for Speech Recognition". *IEEE/ACM Transactions on Audio, Speech, and Language Processing*, Vol. 22, No. 10, pp. 1533–1545. ISSN 2329-9290, 2329-9304. doi:10.1109/TASLP.2014.2339736. URL http://ieeexplore.ieee.org/document/6857341/.

Buitinck, L., Louppe, G., Blondel, M., Pedregosa, F., Mueller, A., Grisel, O., Niculae, V., Prettenhofer, P., Gramfort, A., Grobler, J., Layton, R., Vanderplas, J., Joly, A., Holt, B. and Varoquaux, G., 2013. "API design for machine learning software: experiences from the scikit-learn project". *arXiv:1309.0238 [cs]*. URL http://arxiv.org/abs/1309.0238. ArXiv: 1309.0238.

Calazan, L.B., Moura, F.P., Nascimento, G.C., Bento, T.F.B. and Moreira, R.M., 2021. "Analysis and prediction of equivalent diameter of air bubbles rising in water (submitted)". *Journal of Applied Fluid Mechanics*.

Cheng, Y., Lin, M., Wu, J., Zhu, H. and Shao, X., 2021. "Intelligent fault diagnosis of rotating machinery based on continuous wavelet transform-local binary convolutional neural network". *Knowledge-Based Systems*, Vol. 216, p. 106796. ISSN 09507051. doi:10.1016/j.knosys.2021.106796. URL https://linkinghub.elsevier.com/retrieve/pii/S0950705121000599.

Chiang, L.H., Braatz, R.D. and Russell, E., 2001. *Fault detection and diagnosis in industrial systems*. Advanced textbooks in control and signal processing. Springer, London ; New York. ISBN 978-1-85233-327-0.

de Souza Jr., M.B., 1993. *Redes Neuronais Multicamadas Aplicadas a Modelagem e Controle de Processos Químicos.* Tese de Doutorado, PEQ/COPPE/Universidade Federal do Rio de Janeiro, Rio de Janeiro.

Ge, X., Wang, B., Yang, X., Pan, Y., Liu, B. and Liu, B., 2021. "Fault detection and diagnosis for reactive distillation based on convolutional neural network". *Computers & Chemical Engineering*, Vol. 145, p. 107172. ISSN 00981354. doi:10.1016/j.compchemeng.2020.107172. URL https://linkinghub.elsevier.com/retrieve/pii/S0098135420309741.

Glorot, X., Bordes, A. and Bengio, Y., 2011. "Deep sparse rectifier neural networks". In G. Gordon, D. Dunson and M. Dudík, eds., *Proceedings of the Fourteenth International Conference on Artificial Intelligence and Statistics*. PMLR, Fort Lauderdale, FL, USA, Vol. 15 of *Proceedings of Machine Learning Research*, pp. 315–323. URL http://proceedings.mlr.press/v15/glorot11a.html.

Hirt, C.W. and Nichols, B.D., 1981. "Volume of fluid (VOF) method for the dynamics of free boundaries". *Journal of Computational Physics*, Vol. 39, No. 1, pp. 201–225. ISSN 0021-9991. doi:10.1016/0021-9991(81)90145-5. URL https://www.sciencedirect.com/science/article/pii/0021999181901455.

Isermann, R., 2006. *Fault-diagnosis systems: an introduction from fault detection to fault tolerance*. Springer, Berlin ; New York. ISBN 978-3-540-24112-6. OCLC: ocm61703226.

Jiao, J., Zhao, M., Lin, J. and Liang, K., 2020. "A comprehensive review on convolutional neural network in machine fault diagnosis". *Neurocomputing*, Vol. 417, pp. 36–63. ISSN 09252312. doi:10.1016/j.neucom.2020.07.088. URL https://linkinghub.elsevier.com/retrieve/pii/S092523122031225X.

Kingma, D.P. and Ba, J., 2017. "Adam: A Method for Stochastic Optimization". *arXiv:1412.6980 [cs]*. URL http://arxiv.org/abs/1412.6980. ArXiv: 1412.6980.

Krizhevsky, A., Sutskever, I. and Hinton, G.E., 2012. "ImageNet Classification with Deep Convolutional Neural Networks". *Advances in Neural Information Processing Systems*, Vol. 25, pp. 1097–1105. URL

https://proceedings.neurips.cc/paper/2012/hash/c399862d3b9d6b76c8436e924a68c45b-Abstract.html.

Launder, B.E. and Spalding, D.B., 1974. "The numerical computation of turbulent flows". *Computer Methods in Applied Mechanics and Engineering*, Vol. 3, No. 2, pp. 269–289. ISSN 0045-7825. doi:10.1016/0045-7825(74)90029-2. URL https://www.sciencedirect.com/science/article/pii/0045782574900292.

LeCun, Y., Boser, B., Denker, J.S., Henderson, D., Howard, R.E., Hubbard, W. and Jackel, L.D., 1989. "Backpropagation applied to handwritten zip code recognition". *Neural Computation*, Vol. 1, No. 4, pp. 541–551. ISSN 0899-7667. doi:10.1162/neco.1989.1.4.541. URL https://doi.org/10.1162/neco.1989.1.4.541.

LeCun, Y., Bengio, Y. and Hinton, G., 2015. "Deep learning". *Nature*, Vol. 521, No. 7553, pp. 436–444. ISSN 1476-4687. doi:10.1038/nature14539. URL https://www.nature.com/articles/nature14539. Number: 7553 Publisher: Nature Publishing Group.

Nazir, M., Khan, F., Amyotte, P. and Sadiq, R., 2008. "Subsea Release of Oil from a Riser: An Ecological Risk Assessment". *Risk Analysis*, Vol. 28, No. 5, pp. 1173–1196. ISSN 1539-6924. doi:https://doi.org/10.1111/j.1539-6924.2008.01136.x. URL https://onlinelibrary.wiley.com/doi/abs/10.1111/j.1539-6924.2008.01136.x. _eprint: https://onlinelibrary.wiley.com/doi/pdf/10.1111/j.1539-6924.2008.01136.x.

Olsen, J.E. and Skjetne, P., 2016. "Current understanding of subsea gas release: A review". *The Canadian Journal of Chemical Engineering*, Vol. 94, No. 2, pp. 209–219. ISSN 00084034. doi:10.1002/cjce.22345. URL http://doi.wiley.com/10.1002/cjce.22345.

Petraglia, F., 2017. *Classification of Underwater Pipeline Events using Deep Convolutional NeuralNetworks*. Ph.D. thesis, COPPE/Universidade Federal do Rio de Janeiro, Rio de Janeiro.

Schäfer, J., Schmitt, P., Hlawitschka, M.W. and Bart, H., 2019. "Measuring Particle Size Distributions in Multiphase Flows Using a Convolutional Neural Network". *Chemie Ingenieur Technik*, Vol. 91, No. 11, pp. 1688–1695. ISSN 0009-286X, 1522-2640. doi:10.1002/cite.201900099. URL https://onlinelibrary.wiley.com/doi/10.1002/cite.201900099.

Sokolova, M. and Lapalme, G., 2009. "A systematic analysis of performance measures for classification tasks". *Information Processing & Management*, Vol. 45, No. 4, pp. 427–437. ISSN 03064573. doi:10.1016/j.ipm.2009.03.002. URL https://linkinghub.elsevier.com/retrieve/pii/S0306457309000259.

Sun, X., Shi, J., Liu, L., Dong, J., Plant, C., Wang, X. and Zhou, H., 2018. "Transferring deep knowledge for object recognition in Low-quality underwater videos". *Neurocomputing*, Vol. 275, pp. 897–908. ISSN 0925-2312. doi:10.1016/j.neucom.2017.09.044. URL http://www.sciencedirect.com/science/article/pii/S0925231217315631.

Tharwat, A., 2020. "Classification assessment methods". *Applied Computing and Informatics*, Vol. ahead-of-print, No. ahead-of-print. ISSN 2634-1964, 2210-8327. doi:10.1016/j.aci.2018.08.003. URL https://www.emerald.com/insight/content/doi/10.1016/j.aci.2018.08.003/full/html.

Venkatasubramanian, V., Rengaswamy, R. and Kavuri, S.N., 2003a. "A review of process fault detection and diagnosis". *Computers & Chemical Engineering*, Vol. 27, No. 3, pp. 313–326. ISSN 00981354. doi:10.1016/S0098-1354(02)00161-8. URL https://linkinghub.elsevier.com/retrieve/pii/S0098135402001618.

Venkatasubramanian, V., Rengaswamy, R., Kavuri, S.N. and Yin, K., 2003b. "A review of process fault detection and diagnosis". *Computers & Chemical Engineering*, Vol. 27, No. 3, pp. 327–346. ISSN 00981354. doi:10.1016/S0098-1354(02)00162-X. URL https://linkinghub.elsevier.com/retrieve/pii/S009813540200162X.

Venkatasubramanian, V., Rengaswamy, R., Yin, K. and Kavuri, S.N., 2003c. "A review of process fault detection and diagnosis". *Computers & Chemical Engineering*, Vol. 27, No. 3, pp. 293–311. ISSN 00981354. doi:10.1016/S0098-1354(02)00160-6. URL https://linkinghub.elsevier.com/retrieve/pii/S0098135402001606.

Wang, X., Jiao, J., Yin, J., Zhao, W., Han, X. and Sun, B., 2019. "Underwater sonar image classification using adaptive weights convolutional neural network". *Applied Acoustics*, Vol. 146, pp. 145–154. ISSN 0003682X. doi:10.1016/j.apacoust.2018.11.003. URL https://linkinghub.elsevier.com/retrieve/pii/S0003682X17311532.

Wu, H. and Zhao, J., 2018. "Deep convolutional neural network model based chemical process fault diagnosis". *Computers & Chemical Engineering*, Vol. 115, pp. 185–197. ISSN 00981354. doi:10.1016/j.compchemeng.2018.04.009. URL https://linkinghub.elsevier.com/retrieve/pii/S0098135418302990.

Zhang, J., Sun, Y., Guo, L., Gao, H., Hong, X. and Song, H., 2020. "A new bearing fault diagnosis method based on modified convolutional neural networks". *Chinese Journal of Aeronautics*, Vol. 33, No. 2, pp. 439–447. ISSN 10009361. doi:10.1016/j.cja.2019.07.011. URL https://linkinghub.elsevier.com/retrieve/pii/S100093611930278X.

7. RESPONSIBILITY NOTICE

The authors are solely responsible for the printed material included in this paper.